

ANALYSIS OF A DOUBLE-LAYERED VIVALDI ANTENNA INSIDE A METALLIC ENCLOSURE

Majid OstadRahimi*, Lotfollah Shafai, and Joe LoVetri

Department of Electrical and Computer Engineering, University of Manitoba, Winnipeg, MB R3T 5V6, Canada

Abstract—A double-layered Vivaldi antenna enclosed by a metallic cylindrical cavity is investigated. The antenna is correlated to the same-size circular horn antenna to exploit the equivalent modal distribution of the Vivaldi-cavity antenna. It is shown that the TM_{11} and TE_{11} are the dominant modes and the proposed antenna operates similar to a dual-mode conical horn. The antenna is fabricated and successfully tested. The radiation characteristics, mutual coupling, as well as cross-polarization level are compared to a similarly sized Vivaldi without any metallic enclosure.

1. INTRODUCTION

Slow traveling-wave Vivaldi antennas were introduced in 70's [1, 2]. The antenna is also known as the tapered slot antenna where the tapering can be linear, partially constant, or the original exponential Vivaldi [3]. The gradual tapering maintains a uniform radiating section in terms of the wavelength, thus the operating bandwidth of the antenna is theoretically unlimited. In practice, however, the operating bandwidth of the antenna will be limited due to the transition between the feeding and radiation sections as well as limited size of the antenna [4]. The wide band and integrated features of the Vivaldi makes it a suitable antenna for variety of applications including ultra wide-band [5, 6], millimeter-wave [7, 8], time-domain through-wall radar [9], and microwave imaging applications [10, 11]. Another useful aspect of Vivaldi antenna is its low cross-polarized (X -pol) radiation which is very important in those applications requiring single-polarized radiation. The antenna's X -pol level can be further decreased by employing Double-Layered Vivaldi Antennas (DLVA) [12].

Received 21 October 2013, Accepted 20 November 2013, Scheduled 1 December 2013

* Corresponding author: Majid OstadRahimi (ostadrah@cc.umanitoba.ca).

We have previously utilized an array of 24 DLVAs for an air-based microwave tomography system [12, 13] where the antennas circularly surround an object-of-interest at an even angular spacing. We then designed and implemented a more sophisticated DLVA-based tomography system by equipping the DLVAs with additional active dipole probes. The probes, consisting of p-i-n diodes, collect the fields scattered by the object based on the modulated scattering technique [14]. The p-i-n diodes require biasing wires to be modulated but the wires perturb the fields in the measurement system. The presence of the wires and existing mutual coupling between the Vivaldi antennas result in an unwanted mismatch between the experimental system and its equivalent computational model, also known as the modeling error [15].

To decrease the mutual coupling between the DLVAs as well as *protecting* the antennas from unwanted perturbations in an array configuration, we studied the behavior of the DLVA inside a metallic enclosure, also referred to as a cavity. The proposed antenna is a very suitable antenna for exploiting multi-polarized microwave tomography systems [16]. This study also benefits those applications utilizing large array of Vivaldi antennas [17]. Note that various antennas have been studied inside a cavity including cavity-backed bowtie antenna [18], loop antenna [19], and spiral antenna [20]. However to the best of our knowledge, there is no study on the effect of cavities on Vivaldi antennas. Herein, we correlate the radiated fields to their equivalent mode distribution of a standard conical horn antenna. In order to compare the performance of the antenna, before and after introducing the metallic enclosure, we used in-house DLVAs for this study. We show that the antenna performs similar to a dual-mode conical horn antenna and the mutual coupling between adjacent antennas decreases depending on the polarization configuration.

2. ANTENNA'S DESCRIPTION

A Vivaldi antenna consists of a radiating section and a feeding section. The radiating section is usually symmetric and balanced. The latter one, the feeding section, delivers the energy to the radiating section and requires an implicit or explicit balun geometry to match an unbalanced coaxial feed to the balanced radiating section. We have previously designed and fabricated a DLVA, shown in Figure 1(a), using stripline geometry for the feed section and elliptical tapering for the radiating section. The DLVA was fabricated using two layers of DiClad-527 substrate, each of which 62.5 mil thick, with relative permittivity 2.5. The ground planes of 50 Ω stripline feed are tapered exponentially to

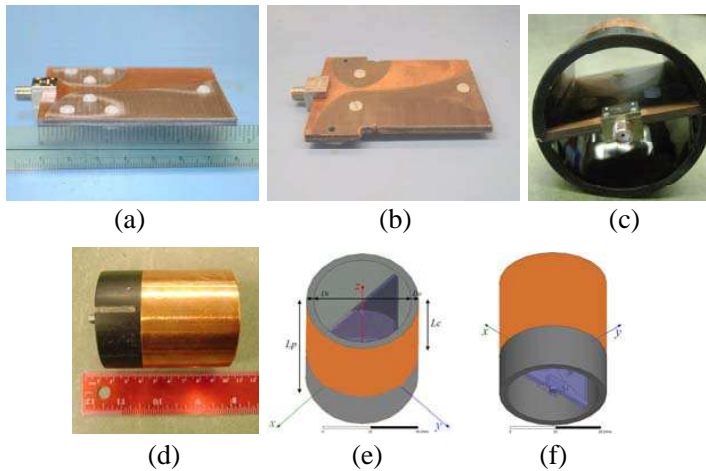


Figure 1. Fabricated antenna's geometry. (a) Photograph of original DLVA. (b) Photograph of the reduced size DLVA. (c) Photograph of DLVA inside cavity from front view. (d) Photograph of the DLVA inside cavity from side view. (e)–(f) Simulated geometry.

the radiating section. The stripline feed is then directly connected to the radiating section. This concludes the description of the original DLVA.

Behavior of the DLVA inside a metallic cylinder is the scope of this paper. The cylinder can be a pure metal, e.g., aluminum or can be made out of non-metallic material covered by a metallic layer. We used off-the-shelf Acrylonitrile-Butadiene-Styrene (ABS) plastic pipe which is made of thermoplastic resin and is widely available and inexpensive. Its permittivity was set to 3 in the simulations. The ABS pipe was then simply covered by a copper tape to create the cavity. Note that the copper tape does not extend to the feed; which is later discussed in more details in the Section 4.1 of this report. The ABS pipes are in standard dimensions. The DLVA's width is 70 mm and the ABS pipe is 60 mm diameter with the thickness of 4 mm. The DLVA was thus cut 7 mm from each side to fit into the ABS pipe. The reduced size DLVA is shown in Figure 1(b). The photographs of the fabricated antenna is shown in Figures 1(c) and (d).

3. MODAL ANALYSIS

Consider a cylindrical open-ended waveguide with perfect-electric conducting walls (PEC), see Figure 2(a). Suppose that the waveguide

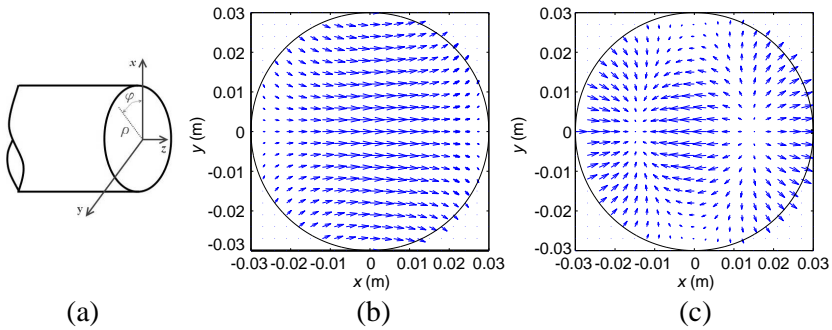


Figure 2. Coordinate system. (a) Cylindrical waveguide. (b) TE_{11} mode field distribution. (c) TM_{11} mode field distribution.

aperture is in the xy -plane and the time-harmonic fields implicitly depend on $e^{j\omega t}$. The field inside and outside the waveguide can be derived from the magnetic vector potential, \mathbf{A} , and electric vector potential, \mathbf{F} , composed of transverse electric (TE) and transverse magnetic (TM) modes. In the TE and TM modes, the electric field and magnetic field are located solely in the transverse plane, respectively. Knowing the fields at the aperture of the antenna, the TE and TM-mode coefficients can be calculated from the formulations provided in this section.

3.1. TE Mode

In the TE mode the sole component of \mathbf{F} is parallel to the z -axis which is expanded in terms of eigen functions as

$$F_z^{\text{TE}} = \sum_{m=-\infty}^{\infty} \sum_{n=1}^{\infty} \alpha_{mn}^{\text{TE}} J_m(\kappa'_{mn}\rho) e^{jm\phi} e^{-j\kappa_z z} \quad (1)$$

$$A_z^{\text{TE}} = 0 \quad (2)$$

where $j^2 = -1$, $\kappa'_{mn} = \chi'_{mn}/a$, $\kappa_{mn}^{\prime 2} = \kappa^2 - \kappa_z^2$, $\kappa^2 = \omega^2 \mu \epsilon$, and $J_m(\cdot)$ is the m th order Bessel function of first kind. The parameters a and χ'_{mn} are the radius of the cylinder and the n th root of $J'_m(\cdot)$ where $J'_m(\nu) = d(J_m(\nu))/d\nu$. Parameters ω , μ , and ϵ are the angular frequency, permeability, and permittivity, respectively. Finally α_{mn} is the mn -mode coefficient.

Longitudinal magnetic field component of the TE mode, H_z , is then calculated from F_z^{TE} and is given by

$$H_z = \sum_{m=-\infty}^{\infty} \sum_{n=1}^{\infty} \alpha_{mn}^{\text{TE}} \left(\frac{-j\kappa_{mn}^{\prime 2}}{\omega\mu\epsilon} \right) J_m(\kappa'_{mn}\rho) e^{jm\phi} e^{-j\kappa_z z}. \quad (3)$$

The $e^{jm\phi}$ can also be expressed in terms of sinusoidal degenerate functions $\begin{bmatrix} \cos(m\phi) \\ \sin(m\phi) \end{bmatrix}$. From orthogonality of derivative of Bessel functions, it can be shown that

$$\int_0^a \rho J_m(\kappa'_{mp}\rho) J_m(\kappa'_{mq}\rho) d\rho = \frac{(\kappa'_{mn}a)^2 - m^2}{2\kappa'^2_{mn}} J_m^2(\kappa'_{mn}a)$$

for $p = q = n$ and the integral vanishes for $p \neq q$. Hence if $H_z(\rho, \phi, z)$ distribution is known at an arbitrary transverse plane, e.g., $z = z_0$, the TE mode coefficients, α_{mn}^{TE} , can be obtained from

$$\alpha_{mn}^{TE} = \frac{\int_0^a \int_0^{2\pi} H_z(\rho, \phi, z_0) J_m(\kappa'_{mn}\rho) \begin{bmatrix} \cos(m\phi) \\ \sin(m\phi) \end{bmatrix} \rho d\rho d\phi}{-j\pi\kappa'^2_{mn} e^{-j\kappa_z z_0} \xi_{mn}} \quad (4)$$

where $\xi_{mn} = \left(\frac{1}{\omega\mu\epsilon}\right) \frac{(\kappa'_{mn}a)^2 - m^2}{2\kappa'^2_{mn}} J_m^2(\kappa'_{mn}a)$.

3.2. TM Mode

The sole component of \mathbf{A} in the TM mode is parallel to the z -axis and is expanded in terms of eigen functions as

$$A_z^{TE} = \sum_{m=-\infty}^{\infty} \sum_{n=1}^{\infty} \alpha_{mn}^{TM} J_m(\kappa_{mn}\rho) e^{jm\phi} e^{-j\kappa_z z} \quad (5)$$

$$F_z^{TE} = 0 \quad (6)$$

where $\kappa_{mn} = \chi_{mn}/a$, $\kappa_{mn}^2 = \kappa^2 - \kappa_z^2$, and χ_{mn} is the n th root of $J_m(\cdot)$.

Longitudinal electric field component of the TM mode, E_z , is then calculated from A_z^{TM} and is given by

$$E_z = \sum_{m=-\infty}^{\infty} \sum_{n=1}^{\infty} \alpha_{mn}^{TM} \left(\frac{-j\kappa_{mn}^2}{\omega\mu\epsilon} \right) J_m(\kappa_{mn}\rho) e^{jm\phi} e^{-j\kappa_z z}. \quad (7)$$

From orthogonality of Bessel functions, it can be shown that

$$\int_0^a \rho J_m(\kappa_{mp}\rho) J_m(\kappa_{mq}\rho) d\rho = \frac{a^2}{2} J_{m+1}^2(\kappa_{mn}a)$$

for $p = q = n$ and the integral vanishes for $p \neq q$. Hence if $E_z(\rho, \phi, z)$ distribution is known at an arbitrary transverse plane, e.g., $z = z_0$, the TM mode coefficients, α_{mn}^{TM} , can be obtained from

$$\alpha_{mn}^{TM} = \frac{\int_0^a \int_0^{2\pi} E_z(\rho, \phi, z_0) J_m(\kappa_{mn}\rho) \begin{bmatrix} \cos(m\phi) \\ \sin(m\phi) \end{bmatrix} \rho d\rho d\phi}{-j\pi\kappa_{mn}^2 e^{-j\kappa_z z_0} \xi_{mn}} \quad (8)$$

where $\xi_{mn} = \left(\frac{1}{\omega\mu\epsilon}\right) \frac{a^2}{2} J_{m+1}^2(\kappa_{mn}a)$.

3.3. Numerical Results

The DLVA-cavity antenna was simulated using Ansys-HFSS [21]. The aperture H_z and E_z fields were then obtained from the numerical simulation at various frequencies from 2 GHz to 11 GHz. The simulation configuration is shown in Figure 1(e). At each frequency, the TE and TM mode coefficients were calculated using Equations (4) and (8), respectively. The results are shown in Figure 3. The dominant modes are TE_{11} and TM_{11} where their field distributions are depicted in Figures 2(b) and (c), respectively.

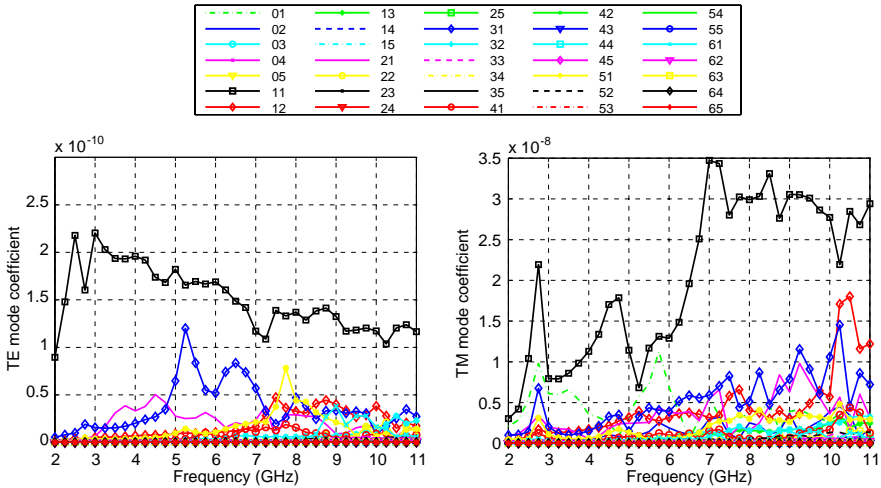


Figure 3. Excited mode coefficients of the DLVA-cavity at various frequencies.

Higher-order modes are also excited however the amplitude of most of these modes are negligible. Since the two TM_{11} and TE_{11} modes are excited simultaneously, the antenna resembles a dual-mode horn antenna also known as the Potter's horn [22].

4. SIMULATIONS AND EXPERIMENTAL RESULTS

In this section we present the measurement results and compare them to simulation results.

4.1. Radiation Pattern

The simulated geometry of the DLVA-cavity antenna is shown in Figure 1(e). The E -plane and H -plane are xz - and yz -planes,

respectively. We measured and simulated the far-field gain pattern of the antenna in both E - and H -planes. The simulated and measured gain patterns of the co-polarized (Co-pol) and X -pol components are shown in Figure 4 in the frequency range of 3.0 GHz to 8.0 GHz.

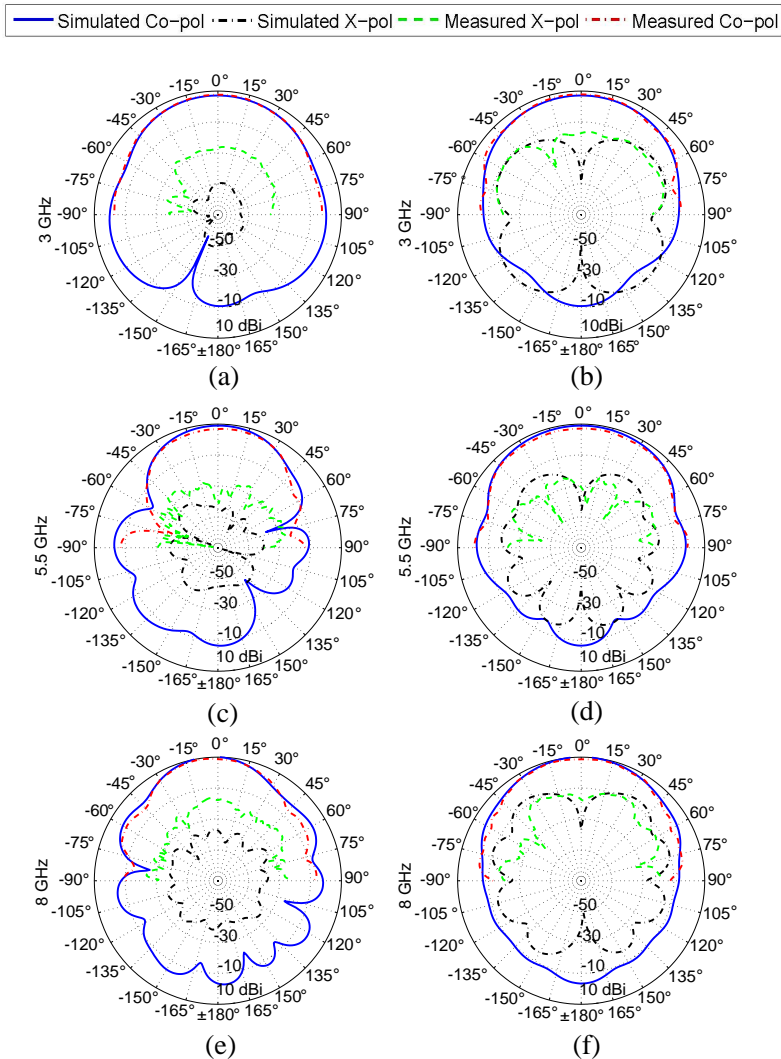


Figure 4. Fabricated antenna’s gain patterns including Co-pol and X -pol components. (a), (c), (e) E -plane, (b), (d), (f) H -plane. Frequencies: (a), (b) 3.0 GHz, (c), (d) 5.5 GHz, and (e), (f) 8.0 GHz.

The measured Co-pol components agree very well with the simulated patterns. The Compact Antenna test range feed has cross polarization around -35 dB, which places a limit on the level of the measured cross polarization. The X -pol components of the DLVA-cavity is below -35 dB. Thus, there is a difference between the simulated and measured X -pol patterns. The difference between the simulated and measured X -pol is more severe in the E -plane which is further discussed in Section 4.2.

Figure 4 shows that there are relatively large radiations from the rear side of the antenna at $\theta = 180^\circ$. The back radiations are due to the geometry of the conductor enclosure. As shown in Figure 1, the conductor enclosure is open at the rear side and it does not fully enclose the rear side of the antenna. The reason for utilizing a partial metallic enclosure is to avoid perturbing the feeding section of the DLVA, thus it remains compatible with air. Without covering the rear side, the input impedance of the antenna remains relatively unchanged and there is no need to change the feeding section. Furthermore, unchanged DLVA

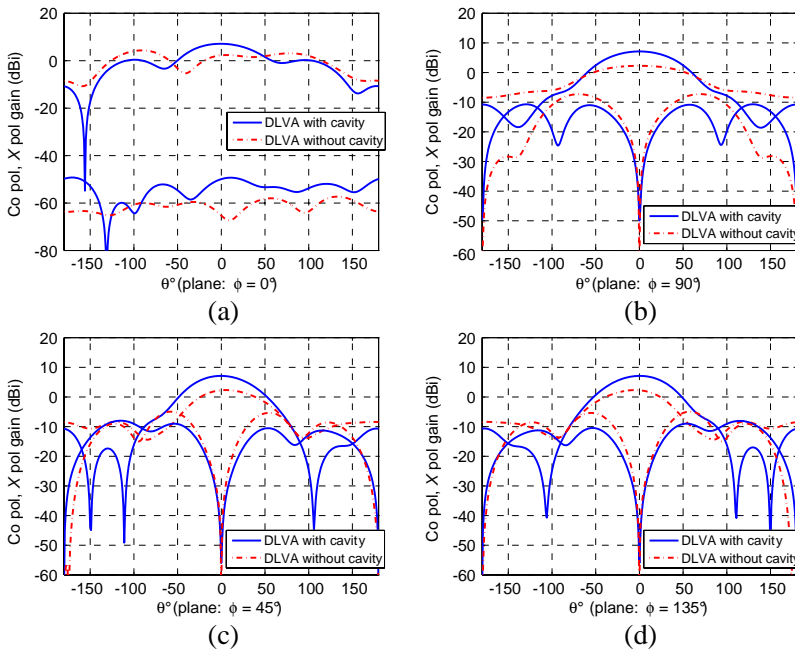


Figure 5. Co-pol and X -pol gain patterns of the Vivaldi antennas (with and without cavity) at 3 GHz, including the E -plane ($\phi = 0^\circ$) and H -plane ($\phi = 90^\circ$).

geometry enables us to compare the performance of the DLVA with and without presence of the metallic enclosure.

We repeated our simulations and measurements for a reduced-size DLVA (see Figure 1(b)), which we refer to as the *DLVA without cavity*. The comparison between the gain patterns of the “DLVA with cavity” and “DLVA without cavity” are shown in Figure 5, Figure 6, and Figure 7 at the frequencies of 3 GHz, 7 GHz, and 11 GHz, respectively.

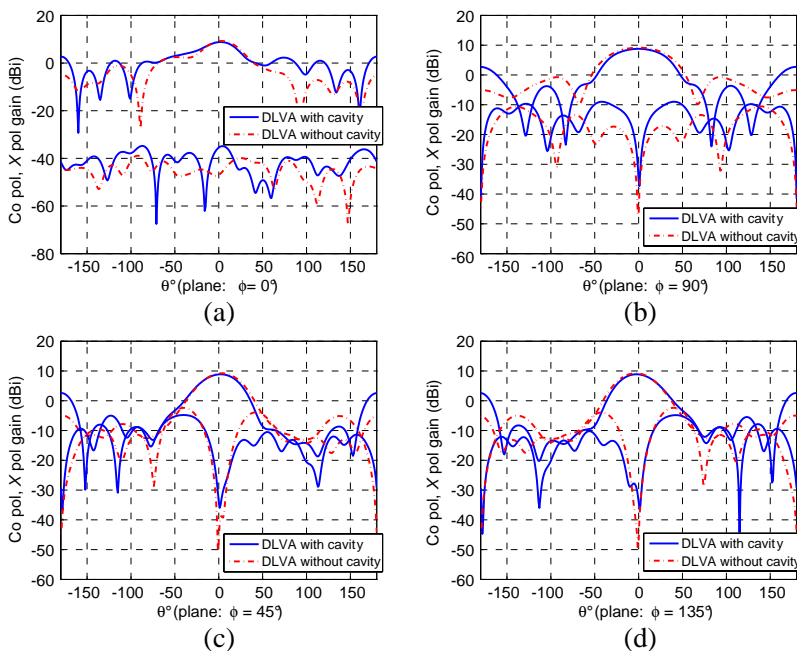


Figure 6. Co-pol and *X*-pol gain patterns of the Vivaldi antennas (with and without cavity) at 7 GHz, including the *E*-plane ($\phi = 0^\circ$) and *H*-plane ($\phi = 90^\circ$).

4.2. Cross-polarized Components and Gain

The radiation pattern of the DLVA-cavity antenna shows that the pattern has minimal angular movement within a large frequency band. Presence of the metallic enclosure maintains the boresight radiation at a precise $\theta = 0^\circ$ angle. Meanwhile, we discussed the modal analysis in Section 3. We showed that the DLVA-cavity antenna is similar to a conical horn with the TE_{11} and TM_{11} modes as the dominant modes.

In our DLVA with cavity antenna, the TM_{11} mode is stronger

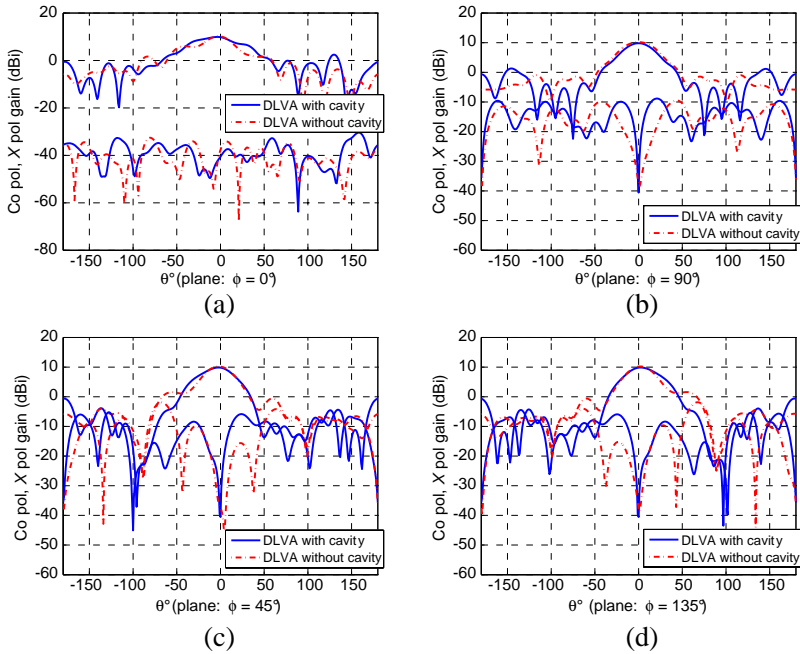


Figure 7. Co-pol and X -pol gain patterns of the Vivaldi antennas (with and without cavity) at 11 GHz, including the E -plane ($\phi = 0^\circ$) and H -plane ($\phi = 90^\circ$).

at frequencies above 7 GHz, see Figure 3. Comparing the results shown in Figure 5, Figure 6, and Figure 7, the E -plane's X -pol component increases significantly from 3 GHz to 11 GHz, whereas it remains unchanged in the H -plane. The aforementioned increase of the X -pol component in the E -plane is due to the stronger excitation of the TM_{11} mode. The radiation characteristics of the TE_{11} and TM_{11} has been fully discussed in [23]. As shown in [22], the TM_{11} mode radiation pattern does not affect the H -plane as it is zero in this plane. It however increases the X -pol radiation in the E -plane which also affects the X -pol component at the $\phi = 45^\circ$ and $\phi = 135^\circ$ planes.

The boresight gain of the three Vivaldi antennas are shown in Figure 8. The gain variation of the DLVA with cavity changes between 8 to 10 dBi at frequencies higher than 4 GHz which is more stable than that in conventional Vivaldi antennas. As shown in Figure 8, stronger excitation of the TM_{11} mode at 7 GHz decreases the gain of the DLVA with cavity.

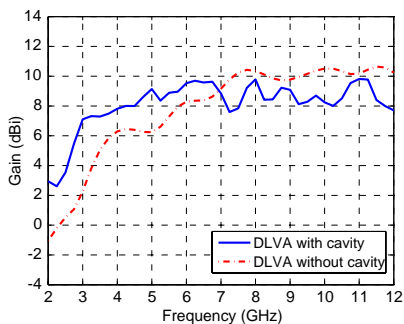


Figure 8. Simulated boresight gain behavior at different frequencies.

4.3. Mutual Coupling and Reflection Coefficient

In those applications utilizing an array of Vivaldi antennas, the mutual coupling between adjacent antennas is important. In most of these applications, reducing the mutual coupling is required. We studied the characteristics of the DLVAs when they are located in a close proximity to each other. For this study, we placed two antennas touching each other with different polarization orientations: 1) the antennas are vertically polarized, 2) the antennas are horizontally polarized, and 3) both antennas are slanted. We repeated this study for a DLVA without cavity. The results are shown in Figure 9, Figure 10, and Figure 11 for the horizontal, vertical and slanted orientations, respectively. The results are discussed in the next section.

Finally, the reflection coefficient of the DLVA with cavity and DLVA without cavity are shown in Figure 12(a) and Figure 12(b), respectively. There is a difference between the simulations and

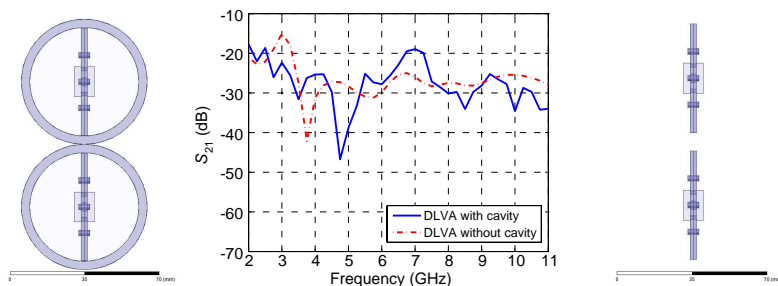


Figure 9. Comparing mutual coupling of horizontally aligned antennas: simulated DLVA with and without cavity.

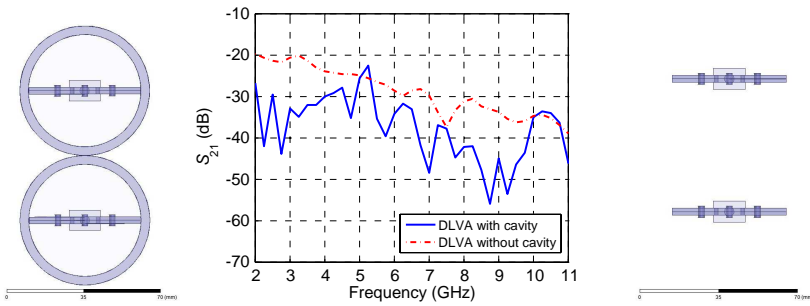


Figure 10. Comparing mutual coupling of vertically aligned antennas: simulated DLVA with and without cavity.

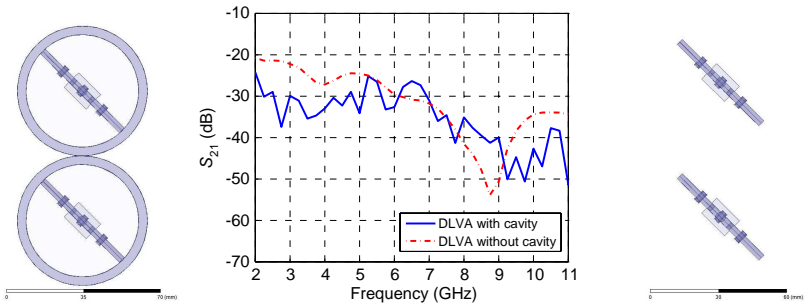


Figure 11. Comparing mutual coupling of slant aligned antennas: simulated DLVA with and without cavity.

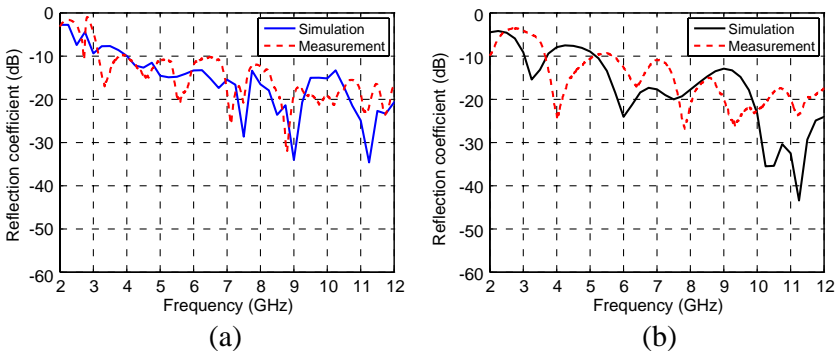


Figure 12. Reflection coefficient of (a) DLVA with cavity and (b) DLVA without cavity.

measurements; which is mostly due to the fabrication [12]. The 10 dB impedance bandwidth of both antennas start at 4 GHz.

5. DISCUSSION AND CONCLUSION

A DLVA is a suitable option for applications requiring integrated broadband antennas, however the antenna's radiation beam moves at different frequencies and the antenna can be easily perturbed by components placed in its proximity. Further, using Vivaldi antennas in array configuration, increases the mutual coupling between adjacent antennas. We investigated the performance of the antenna when enclosed by a metallic cavity. The most important advantage of the metallic enclosure is shielding the Vivaldi from unwanted perturbations which is significantly important in some applications such as multi-polarized microwave tomography systems [16]. The modal analysis of the DLVA-cavity shows that the antenna operates very similar to a dual-mode conical horn. The excitation of the TE_{11} and TM_{11} modes maintains the radiation beam at a precise boresight angle. The gain variations of the DLVA with cavity is lower compared to the similarly-sized DLVA without cavity. In particular, stronger excitation of the TM_{11} mode at higher frequencies, reduces the gain of the DLVA with cavity, see Figure 8. Our analysis shows that X -pol component of the DLVA with cavity is not affected in the H -plane due to the minimal contribution of the TM_{11} mode in the H -plane. On the other hand, excessive TM_{11} mode increases the X -pol component at the E -plane substantially, for instance compare the E -plane's X -pol level of the DLVA with cavity at 7 GHz (Figure 6) and 11 GHz (Figure 7) with that at 3 GHz (Figure 5). Mutual couplings of horizontally aligned DLVAs are similar either with cavity or without cavity. This is due to the fact that the TE_{11} mode is excited and thus the field distribution matches to the antennas aligned horizontally and increases the mutual coupling, see Figure 9. Vertical orientation of the DLVAs, reduces mutual coupling between adjacent antennas when located inside a cavity. As shown in Figure 10, the mutual coupling of the DLVA with cavity is lower than that of the DLVA without cavity at all frequencies except 5.1 GHz. The TE_{31} is excited at about 5.1 GHz (see Figure 3), thus the mutual coupling increases. The modal analysis is very useful to predict the behavior of an antenna inside a cavity. This analysis is also useful for those applications requiring minimum X -pol radiation from a Vivaldi antenna which can be obtained by controlling the modes using metallic perturbations [24].

ACKNOWLEDGMENT

The authors would like to thank Mr. Cory Smit for fabricating the antennas and Mr. Brad Tabachnick for antenna measurements from the University of Manitoba's machine shop and antenna lab, respectively.

REFERENCES

1. Gibson, P., "The Vivaldi aerial," *9th European Microwave Conference*, 101–105, 1979.
2. Lewis, L., M. Fassett, and J. Hunt, "A broadband stripline array element," *IEEE Antennas and Propagation Society International Symposium*, Vol. 12, 335–337, 1974.
3. Yngvesson, K., D. Schaubert, T. Korzeniowski, E. Kollberg, T. Thungren, and J. A. Johansson, "Endfire tapered slot antennas on dielectric substrates," *IEEE Transactions on Antennas and Propagation*, Vol. 33, No. 12, 1392–1400, Dec. 1985.
4. Gazit, E., "Improved design of the Vivaldi antenna," *IEE Proceedings H — Microwaves, Antennas and Propagation*, Vol. 135, No. 2, 89–92, Apr. 1988.
5. Mehdipour, A., K. Mohammadpour-Aghdam, and R. Faraji-Dana, "Complete dispersion analysis of Vivaldi antenna for ultra wideband applications," *Progress In Electromagnetics Research*, Vol. 77, 85–96, 2007.
6. Lai, A., A. Sinopoli, and W. Burnside, "A novel antenna for ultra-wide-band applications," *IEEE Transactions on Antennas and Propagation*, Vol. 40, No. 7, 755–760, 1992.
7. Bai, J., S. Shi, and D. Prather, "Modified compact antipodal Vivaldi antenna for 4–50 GHz UWB application," *IEEE Transactions on Microwave Theory and Techniques*, Vol. 59, No. 4, 1051–1057, 2011.
8. Simons, R. and R. Lee, "On-wafer characterization of millimeter-wave antennas for wireless applications," *IEEE Transactions on Microwave Theory and Techniques*, Vol. 47, No. 1, 92–96, 1999.
9. Yang, Y., Y. Wang, and A. E. Fathy, "Design of compact Vivaldi antenna arrays for UWB see through wall applications," *Progress In Electromagnetics Research*, Vol. 82, 401–418, 2008.
10. Woten, D., M. Hajihashemi, A. Hassan, and M. El-Shenawee, "Experimental microwave validation of level set reconstruction algorithm," *IEEE Transactions on Antennas and Propagation*, Vol. 58, No. 1, 230–233, 2010.

11. Maklad, B., C. Curtis, E. C. Fear, and G. G. Messier, "Neighborhood-based algorithm to facilitate the reduction of skin reactions in radar-based microwave imaging," *Progress In Electromagnetics Research B*, Vol. 39, 115–139, 2012.
12. Ostadrahimi, M., S. Noghianian, L. Shafai, A. Zakaria, C. Kaye, and J. LoVetri, "Investigating a double layer Vivaldi antenna design for fixed array eld measurement," *International Journal of Ultra Wideband Communications and Systems*, Vol. 1, No. 4, 282–290, 2010.
13. Gilmore, C., A. Zakaria, P. Mojabi, M. Ostadrahimi, S. Pistorius, and J. Lo Vetri, "The University of Manitoba microwave imaging repository: A two-dimensional microwave scattering database for testing inversion and calibration algorithms," *IEEE Antennas and Propagation Magazine*, Vol. 53, No. 5, 126–133, Oct. 2011.
14. Ostadrahimi, M., P. Mojabi, S. Noghianian, L. Shafai, S. Pistorius, and J. LoVetri, "A novel microwave tomography system based on the scattering probe technique," *IEEE Transactions on Instrumentation and Measurement*, Vol. 61, No. 2, 379–390, Feb. 2012.
15. Ostadrahimi, M., P. Mojabi, C. Gilmore, A. Zakaria, S. Noghianian, S. Pistorius, and J. LoVetri, "Analysis of incident field modeling and incident/scattered field calibration techniques in microwave tomography," *IEEE Antennas and Wireless Propagation Letters*, Vol. 10, 900–903, 2011.
16. Ostadrahimi, M., A. Zakaria, J. LoVetri, and L. Shafai, "A near-field dual polarized TE-TM microwave imaging system," *IEEE Transactions on Microwave Theory and Techniques*, Vol. 61, No. 3, 1376–1384, 2013.
17. Yang, Y., C. Zhang, and A. Fathy, "Development and implementation of ultra-wideband see-through-wall imaging system based on sampling oscilloscope," *IEEE Antennas and Wireless Propagation Letters*, Vol. 7, 465–468, 2008.
18. Qu, S., J. Li, Q. Xue, and C. Chan, "Wideband cavity-backed bowtie antenna with pattern improvement," *IEEE Transactions on Antennas and Propagation*, Vol. 56, No. 12, 3850–3854, 2008.
19. Li, R., B. Pan, A. Traille, J. Papapolymerou, J. Laskar, and M. Tentzeris, "Development of a cavity-backed broadband circularly polarized slot/strip loop antenna with a simple feeding structure," *IEEE Transactions on Antennas and Propagation*, Vol. 56, No. 2, 312–318, 2008.

20. Ozdemir, T., J. Volakis, and M. Nurnberger, "Analysis of thin multioctave cavity-backed slot spiral antennas," *IEE Proceedings — Microwaves, Antennas and Propagation*, Vol. 146, No. 6. 447–454, 1999,
21. "Ansys-HFSS simulator package," 2012, Online Available: www.ansys.com.
22. Potter, P., "A new horn antenna with suppressed sidelobes and equal beamwidths," *Microwave Journal*, 71, 1963.
23. Silver, S., *Microwave Antenna Theory and Design*, The Institution of Electrical Engineers, Vol. 19. 1984.
24. Olver, A. D., P. Clarricoats, A. Kishk, and L. Shafai, *Microwave Horns and Feeds*, 490, IET, 1994.